Article

Dual Solutions and Stability Analysis of a Hybrid Nanofluid over a Stretching/Shrinking Sheet Executing MHD Flow

Liaquat Ali Lund [1,2] ，**Zurni Omar** [1]，**Ilyas Khan** [3,*] and **El-Sayed M. Sherif** [4,5]

1   School of Quantitative Sciences, Universiti Utara Malaysia, Sintok 06010, Kedah, Malaysia;
    balochliaqatali@gmail.com (L.A.L.); zurni@uum.edu.my (Z.O.)
2   KCAET Khairpur Mir's Sindh Agriculture University, Tandojam Sindh 70060, Pakistan
3   Faculty of Mathematics and Statistics, Ton Duc Thang University, Ho Chi Minh City 72915, Vietnam
4   Center of Excellence for Research in Engineering Materials (CEREM), King Saud University, P.O. Box 800,
    Al-Riyadh 11421, Saudi Arabia; esherif@ksu.edu.sa
5   Electrochemistry and Corrosion Laboratory, Department of Physical Chemistry, National Research Centre,
    El-Behoth St. 33, Dokki, Cairo 12622, Egypt
*   Correspondence: ilyaskhan@tdtu.edu.vn

check for updates

Abstract: In this paper, the unsteady magnetohydrodynamic (MHD) flow of hybrid nanofluid (HNF) composed of $Cu - Al_2O_3$/water in the presence of a thermal radiation effect over the stretching/shrinking sheet is investigated. Using similarity transformation, the governing partial differential equations (PDEs) are transformed into a system of ordinary differential equations (ODEs), which are then solved by using a shooting method. In order to validate the obtained numerical results, the comparison of the results with the published literature is made numerically as well as graphically and is found in good agreements. In addition, the effects of many emerging physical governing parameters on the profiles of velocity, temperature, skin friction coefficient, and heat transfer rate are demonstrated graphically and are elucidated theoretically. Based on the numerical results, dual solutions exist in a specific range of magnetic, suction, and unsteadiness parameters. It was also found that the values of $f''(0)$ rise in the first solution and reduce in the second solution when the solid volume fraction ϕ_{Cu} is increased. Finally, the temporal stability analysis of the solutions is conducted, and it is concluded that only the first solution is stable.

Keywords: dual solutions; stability analysis; HNF; magnetic field; thermal radiation

1. Introduction

Researchers are interested in studying the enhancement of heat transfer due to its significant applications in engineering and industries. The heat transfer of convectional fluids such as ethylene glycol, water, and oil can be utilized in various apparatus of engineering, for instance, devices of electrons and heat exchangers. However, these base liquids keep limited thermal conductivity or, in other words, they have low thermal conductivity. To overcome this shortcoming, engineers, mathematicians, and researchers of various fields attempt to improve thermal conductivity of previously mentioned liquids by including a solitary kind of nanosized particles to form a mixture called 'nanofluid', which was initially presented by Choi and Eastman [1]. It is easily shown from the previous studies that solid nanoparticles possess the ability increase thermal conductivity and the rate of heat transfer of convectional base fluids. Consequently, numerous analysts and thermal experts have carried out investigations in order to enhance the rate of heat transfer of nanofluid for various perspectives, numerically as well as experimentally. For instance, the examination of the single-phase models of

nanofluids was established by Tiwari and Das [2]. This model has been constructed by considering a solid volume fraction of nanoparticles in the base fluid, and, later, the governing equations have been solved numerically by employing the finite volume method. As a result, this model has been widely considered by many scientists, engineers, and mathematicians, such as Benzema et al. [3], Dero et al. [4], Lund et al. [5,6], Dogonchi, et al. [7,8], Amini, et al. [9], Zaib et al. [10], Raza et al. [11], Rasool et al. [12,13], Dinarvand et al. [14], and Roşca, et al. [15] to investigate different types of flow. Furthermore, to keep the demand of the high heat transfer rate from industries and other sectors, researchers have introduced a new kind of the nanofluid by considering the two different types of the solid particles in the single convectional base fluid. This kind of nanofluid is known as a hybrid nanofluid [16]. It is worth mentioning that thermal conductivity of regular base fluid in hybrid nanofluid is higher than in simple nanofluid.

Due to this nice property, studies of different types of hybrid nanofluids have gained attention. Devi and Devi [17] examined the $Cu - Al_2O_3/$ water hybrid nanofluid. The obtained numerical results were compared with the experimental results of Suresh et al. [18] and were found in excellent agreement. Toghraie et al. [19] further adopted this model for the $ZnO - TiO_2/EG$ hybrid nanofluid. Meanwhile, Moghadassi et al. [20] studied the $Al_2O_3 - Cu/$ water base hybrid nanofluid numerically and found that "for the hybrid nanofluids, the average Nusselt number increase was 4.73% and 13.46% in compared to Al_2O_3 water and pure water, respectively". Moreover, this model has been widely employed by many researchers, such as Hayat et al. [21], Saba et al. [22], Acharya et al. [23], Afridi et al. [24], Shafiq et al. [25,26], and Manh et al. [27]. Furthermore, Khashi'ie et al. [28] found dual solutions of magnetohydrodynamic (MHD) flow of a hybrid nanofluid in the presence of Joule heating and noticed that higher values of Eckert number do not affect boundary layer separation. Lund et al. [29] studied hybrid nanofluids by considering copper and alumina as solid particles with water as a base fluid. Dual solutions were noticed in the presence of high suction. Dual solutions of a hybrid nanofluid over a vertical thin needle were investigated by Waini et al. [30]. They performed a stability analysis on dual solutions and discovered that only the first solution is stable. Later, Waini et al. [31] considered an unsteady flow of hybrid nanofluid over a stretching/shrinking surface and found that dual solutions appeared in certain ranges of an unsteadiness parameter.

This paper is an extension of the study carried out by Waini et al. [31] by considering the unsteady magnetohydrodynamic (MHD) flow of the $Cu - Al_2O_3/$ water hybrid nanofluid in the presence of thermal radiation over the stretching/shrinking parameter. A model of Tiwari and Das [2] is used to deal with governing equations by including two solid nanoparticles, namely copper (Cu) and alumina (Al_2O_3), with water as a base fluid. To the best of authors' knowledge and based on a survey of previous literature, this kind of study has not been investigated.

2. Problem Formulation

Let us consider an unsteady MHD incompressible flow of the $Cu - Al_2O_3/$ water nanofluid flow on a stretching/shrinking sheet in the presence of thermal radiation effect. Figure 1 shows the physical model and coordinate system of the concerned problem. The velocity of wall mass transfer is $v_w(x) = -\left(\frac{\vartheta_f c}{(1-\varepsilon t)}\right)^{\frac{1}{2}} f(\eta)$ where c is a positive constant. It is also assumed that the flow is subjected to a transverse magnetic field of strength $B = \frac{B_0}{(1-\varepsilon t)^{1/2}}$ where B_0 is the constant applied magnetic field. By including the considered assumptions, the equation of mass, momentum, and energy in the form of a boundary layer are expressed in Tiwari and Das' model [2], as below:

$$\frac{\partial u}{\partial x} + \frac{\partial v}{\partial y} = 0 \tag{1}$$

$$\frac{\partial u}{\partial t} + u\frac{\partial u}{\partial x} + v\frac{\partial u}{\partial y} = \frac{\mu_{hnf}}{\rho_{hnf}}\frac{\partial^2 u}{\partial y^2} - \frac{\sigma^* B^2 u}{\rho_{hnf}} \tag{2}$$

$$\frac{\partial T}{\partial t} + u\frac{\partial T}{\partial x} + v\frac{\partial T}{\partial y} = \left[\frac{k_{hnf}}{(\rho c_p)_{hnf}} + \frac{16\sigma_1 T_\infty^3}{3k^*(\rho c_p)_{hnf}}\right]\frac{\partial^2 T}{\partial y^2} \tag{3}$$

subject to the following boundary conditions:

$$\begin{cases} t < 0,\ u = v = 0, T = T_\infty \\ t \geq 0, v = v_w,\ u = \lambda u_w, T = T_w\ at\ y = 0 \\ u \to 0,\ T \to T_\infty\ as\ y \to \infty \end{cases} \tag{4}$$

where $u_w(x,t) = = \frac{cx}{(1-\varepsilon t)}$ is the velocity of the surface. In the current study, thermophoresis properties of Waini et al. [31] are adopted. These properties of hybrid nanofluid are presented in Tables 1 and 2.

In order to reduce the governing equations into a system of ordinary differential equations (ODEs), the following similarity transformation variables are employed:

$$\eta = \left(\frac{c}{\vartheta_f(1-\varepsilon t)}\right)^{\frac{1}{2}} y,\ u = \frac{cx}{(1-\varepsilon t)}f\prime(\eta),\ v = -\left(\frac{\vartheta_f c}{(1-\varepsilon t)}\right)^{\frac{1}{2}} f(\eta), \theta(\eta) = \frac{T-T_\infty}{T_w - T_\infty} \tag{5}$$

Substituting Equation (5) in Equations (1)–(3), Equation (1) is definitely fulfilled, and Equations (2)–(3) take the accompanying dimensionless form of ODEs:

$$f''' + \xi_1\left\{ff'' - f\prime^2 - A(0.5\eta f'' + f')\right\} - \xi_2 M f' = 0 \tag{6}$$

$$\frac{1}{\xi_3 Pr}\left[(k_{hnf}/k_f) + \frac{4Rd}{3}\right]\theta'' + f\theta' - 0.5A\eta\theta' = 0 \tag{7}$$

subject to the following boundary conditions:

$$\begin{cases} f(0) = S, f'(0) = \lambda,\ \theta(0) = 1 \\ f'(\eta) \to 0, \theta(\eta) \to 0\ as\ \eta \to \infty \end{cases} \tag{8}$$

The reduced quantities are expressed as $A = \frac{\varepsilon}{c}, M = \frac{\sigma^* B_0^2}{c\,\rho_f}, Pr = \frac{\vartheta_f}{\alpha_f}, Rd = \frac{4\sigma_1 T_\infty^3}{k^* k_f}$.

$$\begin{cases} \xi_1 = \left(1 - \phi_{Al_2O_3}\right)^{2.5}(1 - \phi_{Cu})^{2.5}\left\{(1 - \phi_{Cu})\left[1 - \phi_{Al_2O_3} + \phi_{Al_2O_3}\left(\frac{\rho_{Al_2O_3}}{\rho_f}\right)\right] + \phi_{Cu}\left(\frac{\rho_{Cu}}{\rho_f}\right)\right\} \\ \xi_2 = (1 - \phi_{Cu})^{2.5}\left(1 - \phi_{Al_2O_3}\right)^{2.5} \\ \xi_3 = \left\{(1 - \phi_{Cu})\left[1 - \phi_{Al_2O_3} + \phi_{Al_2O_3}\frac{(\rho c_p)_{Al_2O_3}}{(\rho c_p)_f}\right] + \phi_{Cu}\frac{(\rho c_p)_{Cu}}{(\rho c_p)_f}\right\} \end{cases} \tag{9}$$

The physical quantities of attention are the skin friction coefficient C_f and the local Nusselt number Nu_x, which are expressed as follows:

$$C_f = \frac{\mu_{hnf}}{\rho_f u_w^2}\left(\frac{\partial u}{\partial y}\right)|y = 0,\ Nu_x = -\frac{xk_{hnf}}{k_f(T_w - T_\infty)}\left(\frac{\partial T}{\partial y}\right)|y = 0 \tag{10}$$

Applying Equation (5) in Equation (10), leads to:

$$\sqrt{Re}C_f = \frac{1}{\left(1 - \phi_{Al_2O_3}\right)^{2.5}(1 - \phi_{Cu})^{2.5}}f''(0);\ \sqrt{\frac{1}{Re}}Nu_x = -\frac{k_{hnf}}{k_f}\left[1 + \frac{4Rd}{3}\right]\theta'(0) \tag{11}$$

where $Re = \frac{xu_w}{\vartheta_f}$ is the local Reynold number.

(a) Stretching Sheet $\lambda > 0$ (b) Shrinking Sheet $\lambda < 0$
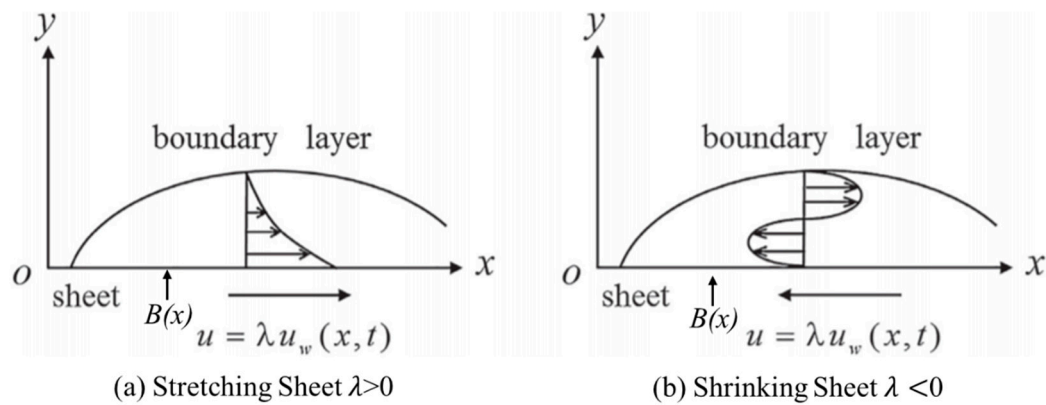
Figure 1. Physical models and coordinate systems.

3. Stability Analysis

In order to perform a temporal analysis of the solutions' stability, introducing a new dimensionless time-dependent similarity transformation variable is required, as recommended by Merkin [32], Dero et al. [33,34], and Lund et al. [35–37]. Letting $\tau = \frac{ct}{(1-\varepsilon t)}$ yields the following new similarity transformation variables:

$$
\begin{cases}
u = \frac{cx}{(1-\varepsilon t)}\frac{\partial f(\eta,\tau)}{\partial \eta}, \ v = -\left(\frac{\vartheta_f c}{(1-\varepsilon t)}\right)^{\frac{1}{2}} f(\eta,\tau), \theta(\eta,\tau) = \frac{T-T_\infty}{T_w-T_\infty} \\
\eta = \left(\frac{c}{\vartheta_f(1-\varepsilon t)}\right)^{\frac{1}{2}} y; \ \tau = \frac{ct}{(1-\gamma t)}
\end{cases}
\tag{12}
$$

Substituting Equation (12) in Equations (2) and (3) leads to:

$$
\frac{\partial^3 f}{\partial \eta^3} + \xi_1 \left\{ f\frac{\partial^2 f}{\partial \eta^2} - \left(\frac{\partial f}{\partial \eta}\right)^2 - A\left(0.5\eta\frac{\partial^2 f}{\partial \eta^2} + \frac{\partial f}{\partial \eta}\right) - (1 + A\tau)\frac{\partial^2 f}{\partial \tau \partial \eta} \right\} - \xi_2 M\frac{\partial f}{\partial \eta} = 0
\tag{13}
$$

$$
\frac{1}{\xi_3 Pr}\left[(k_{hnf}/k_f) + \frac{4Rd}{3}\right]\frac{\partial^2 \theta}{\partial \eta^2} + f\frac{\partial \theta}{\partial \eta} - 0.5A\eta\frac{\partial \theta}{\partial \eta} - (1 + A\tau)\frac{\partial \theta}{\partial \tau} = 0
\tag{14}
$$

subject to the following boundary conditions:

$$
\begin{cases}
f(0,\tau) = S, \ \frac{\partial f(0,\tau)}{\partial \eta} = \lambda, \theta(0,\tau) = 1 \\
\frac{\partial f\eta(,\tau)}{\partial \eta} = \theta(\eta,\tau) = 0 \ as \ \eta \to \infty
\end{cases}
\tag{15}
$$

To check the stability of the steady flow solutions, where $f(\eta) = f_0(\eta), \theta(\eta) = \theta_0(\eta)$, and $\varnothing(\eta) = \varnothing_0(\eta)$, the following boundary value problem (8)-(11) must be satisfied:

$$
\begin{cases}
f(\eta,\tau) = f_0(\eta) + e^{-\gamma\tau}F(\eta,\tau) \\
\theta(\eta,\tau) = \theta_0(\eta) + e^{-\gamma\tau}G(\eta,\tau)
\end{cases}
\tag{16}
$$

where $F(\eta)$ and $G(\eta)$ are small relatives of $f_0(\eta)$ and $\theta_0(\eta)$, respectively, and γ is an unknown eigenvalue parameter, which need to be determined. Substituting Equation (16) in Equations (13)–(14) by considering $\tau = 0$, gives the following linearized eigenvalue problem:

$$
F_0''' + \xi_1\{f_0 F_0'' - 2f_0'F_0' + F_0 f_0'' - A(0.5\eta F_0'' + F_0') + F_0'\} - \xi_2 M F_0' = 0
\tag{17}
$$

$$
\frac{1}{\xi_3 Pr}\left[(k_{hnf}/k_f) + \frac{4Rd}{3}\right]G_0'' + f_0 G_0' + F_0\theta_0' - 0.5\eta A G_0' + G_0 = 0
\tag{18}
$$

subject to the following boundary conditions:

$$\begin{cases} F_0(0) = 0, \ F_0'(0) = 0, \ G_0(0) = 0 \\ F_0'(\eta) \to 0, \ G_0(\eta) \to 0 \ as \ \eta \to \infty \end{cases} \tag{19}$$

According to Haris et al. [38] and Khashi'ie et al. [39], one boundary condition has to be relaxed in order to obtain the value(s) of the smallest eigenvalue. It should be noted that this relaxation in boundary condition does not affect the results [40]. In this particular problem, $F_0'(\eta) \to 0$ as $\eta \to \infty$ is relaxed into $F_0''(0) = 1$.

4. Result and Discussion

In this section, Equations (6) and (7) with boundary conditions (8) have been solved numerically by employing the shooting method in Maple software. The shooting method has been employed by many researchers [41–44]. As suggested by Devi and Deci [17], the solid volume fraction $\phi_{Al_2O_3} = 0.1$ is kept as a constant in many graphs. Furthermore, the solid volume fraction ϕ_{Cu} is added in order to make the $Cu - Al_2O_3$/ water hybrid nanofluid. As recommended by Dero et al. [4] and Iqbal et al. [45], the Prandtl number $Pr = 6.2$ is kept as constant and employed to produce the results of the current study. Table 3 shows the comparison of the numerical values of $f''(0)$ and $-\theta'(0)$ with the published results of waini et al. [31] for Cu–water nanofluid. It is worth mentioning that Waini et al. [31] used the 3-stage Labatto IIIa formula in a BVP4C solver to solve the resultant similarity equations. It is found that the current results show outstanding agreement with the results of Waini et al. [31]. Therefore, it can be concluded that the accuracy of the present method is fine, and it can be used in this study. Figure 2 is demonstrated for the comparison purpose in order to check the accuracy of the used method. It is observed that the critical values of the current study have a good agreement with the critical values of published paper (allude Figure 6 in Waini et al. [31]). After comparison, this method can be used confidently in this problem.

Figures 3 and 4 show the variation of $f''(0)$ and $-\theta'(0)$ against A for $\phi_{Cu} = 0.001,\ 0.01,$ and 0.1. By keeping A fixed, an expansion of ϕ_{Cu} creates a reduction in the heat transfer rate, which implies that the heat transfer coefficient is decreased on the sheet, while an opposite nature is observed for the $f''(0)$ in the second solution. On the other hand, the coefficient of skin friction decreases in the first solution. Moreover, it is noticed that multiple solutions exist for $A > A_c$, whereas no solution exists for $A < A_c$. It is worth mentioning here that A_c is the critical value where multiple solutions exist. Variations of $f''(0)$ and $-\theta'(0)$ along M for numerous values of ϕ_{Cu} were drawn in Figures 5 and 6, respectively. It is observed from them that when the solid volume fraction ϕ_{Cu} increases the values of the critical point of M are also increased. Furthermore, $M_{c1} = 0.4492,\ M_{c2} = 0.3912$ are the respective critical values of M for $\phi_{Cu} = 0.001$ and 0.01. It is examined that the critical values of M get smaller for higher values of the solid volume fraction ϕ_{Cu}, which is the physical reason of the extension of the thickness of boundary layer separation. Moreover, it can be seen that the values of $f''(0)$ rises in the first solution and reduces in the second solution when the solid volume fraction ϕ_{Cu} is increased. In the meantime, the rate of heat transfer decreases for the unstable solution and increases for the stable solution with the increasing of ϕ_{Cu}.

In detail, Figures 7 and 8 show the variation of $f''(0)$ and $-\theta'(0)$ with A for the numerous values of the mass suction parameter S. It is observed that the domain of the solutions increases along the critical value of A, moving to one side when the mass suction parameter S is decreased. In light of our calculations, $A_{c1} = -10.1708,\ A_{c2} = -7.2207,$ and $A_{c3} = -5.2042$ are the respective critical values of A for $S = 1.8,\ 1.75$ and 1.7. At the same time, it is examined that the smaller critical value is for $S = 1.8$ as compared to $S = 1.75$ and $S = 1.7$. Henceforth, boundary layer separation is delayed for the higher values of the mass suction S. In addition, the coefficient of skin friction increases in the first solution with the developing of S, whereas it declines in the second solution. The expanding of S prompts to rise the effect of the heat transfer rate $-\theta'(0)$ in both solutions. Figures 9 and 10 demonstrate the variation

of $f''(0)$ and $-\theta'(0)$ with S for the numerous values of ϕ_{Cu}. It can be found that the increments in ϕ_{Cu} lead to smaller critical values of S_c. According to our computation, $S_{c1} = 1.7886$, $S_{c2} = 1.78234$, and $S_{c3} = 1.7496$ are the respective critical values of S for $\phi_{Cu} = 0.001$, 0.01, and 0.1. Furthermore, the heat transfer rate rises in both solutions for the higher values of the mass suction S. This is due to fact that mass suction S helps the molecules of the hybrid nanofluid to transfer the heat effectively. On the other hand, $f''(0)$ increases (decreases) in the first (second) solution when ϕ_{Cu} is enhanced.

Figures 11 and 12 illustrate the profiles of velocity $f'(\eta)$ and the temperature $\theta(\eta)$ for S. It was demonstrated that the rise in S decreases the velocity of the fluid in the first solution but it increases the velocity of the fluid in the second solution. On the other hand, it is perceived that the temperature of fluid decreases with the expansion of the mass suction S. The effect of the thermal radiation parameter on $\theta(\eta)$ is shown in Figure 13. It can be noticed that the thickness of the thermal boundary layer, as well as temperature of the fluid, increases with the increasing values of Rd.

Finally, the linearized eigenvalue Equations (17) and (18) have been solved using a 3-stage Labatto IIIa formula in a BVP4C solver in MATLAB 2017b. The results of the stability analysis of the solutions are demonstrated graphically in Figure 14. It can be easily observed from the figure that the initial decay of disturbance is denoted by the positive value of γ and a stable flow, while the initial growth of disturbance is indicated by the negative values of γ and an unstable flow. Additionally, it is noticed that γ tends to zero at the critical values of A from both solutions.

Table 1. Thermophysical properties of the hybrid nanofluid [46].

Properties	Hybrid Nanofluid
Dynamic viscosity	$\mu_{hnf} = \dfrac{\mu_f}{\left(1-\phi_{Al_2O_3}\right)^{2.5}\left(1-\phi_{Cu}\right)^{2.5}}$
Density	$\rho_{hnf} = (1-\phi_{Cu})\left[\left(1-\phi_{Al_2O_3}\right)\rho_f + \phi_{Al_2O_3}\rho_{Al_2O_3}\right] + \phi_{Cu}\rho_{Cu}$
Thermal conductivity	$k_{hnf} = \dfrac{k_{Cu} + 2k_{nf} - 2\phi_{Cu}\left(k_{nf} - k_{Cu}\right)}{k_{Cu} + 2k_{nf} + \phi_{Cu}\left(k_{nf} - k_{Cu}\right)} \times \left(k_{nf}\right)$ where $k_{nf} = \dfrac{k_{Al_2O_3} + 2k_f - 2\phi_{Al_2O_3}\left(k_f - k_{Al_2O_3}\right)}{k_{Al_2O_3} + 2k_f + \phi_{Al_2O_3}\left(k_f - k_{Al_2O_3}\right)} \times \left(k_f\right)$
Heat capacity	$\left(\rho c_p\right)_{hnf} = (1-\phi_{Cu})\left[\left(1-\phi_{Al_2O_3}\right)\left(\rho c_p\right)_f + \phi_{Al_2O_3}\left(\rho c_p\right)_{Al_2O_3}\right] + \phi_{Cu}\left(\rho c_p\right)_{Cu}$

Table 2. The thermo physical properties of the base fluid (water) and the nanoparticles [47,48].

Fluids	ρ	c_p (J/kg K)	k (W/m K)
Alumina (Al_2O_3)	3970	765	40
Copper (Cu)	8933	385	400
Water (H_2O)	997.1	4179	0.613

Table 3. Values of $f''(0)$ and $\theta'(0)$ for the Cu–water nanofluid ($\phi_{Cu} = 0.2$) with various values of A when $M = Rd = 0$, $S = 2.1$, $Pr = 6.2$, and $\lambda = -1$.

A	$\phi_{Al_2O_3}$	$f''(0)$				$-\theta'(0)$			
		Waini	[31]	Present	Results	Waini	[31]	Present	Results
		1st Soln	2nd Soln	1st Soln	2nd Soln	1st Soln	2nd Soln	1st Soln	2nd Soln
−1	0	2.194247	−1.491281	2.19424658	−1.49128119	7.073680	6.884548	7.0736798	6.88454793
−1	0.1	–	–	1.60888878	−0.69818494	–	–	5.2238150	5.0737595
−3	0	1.521197	−4.144746	1.52119229	−4.14474572	7.497151	7.296176	7.4971508	7.2961762
−3	0.1	–	–	0.83697819	−2.53135605	–	–	5.6316794	5.4925121
−5	0	0.844435	−6.431507	0.84443506	−6.43150738	7.858446	7.657801	7.8584457	7.6578012
−5	0.01	–	–	0.77597819	−6.20435575	–	–	7.6375695	7.4426329
−9	0	−0.517287	−10.58983	−0.51728551	−10.5898303	8.473316	8.277676	8.4733163	8.27767616
−9	0.01	–	–	−0.60021181	−10.2417356	–	–	8.24709639	8.05819003
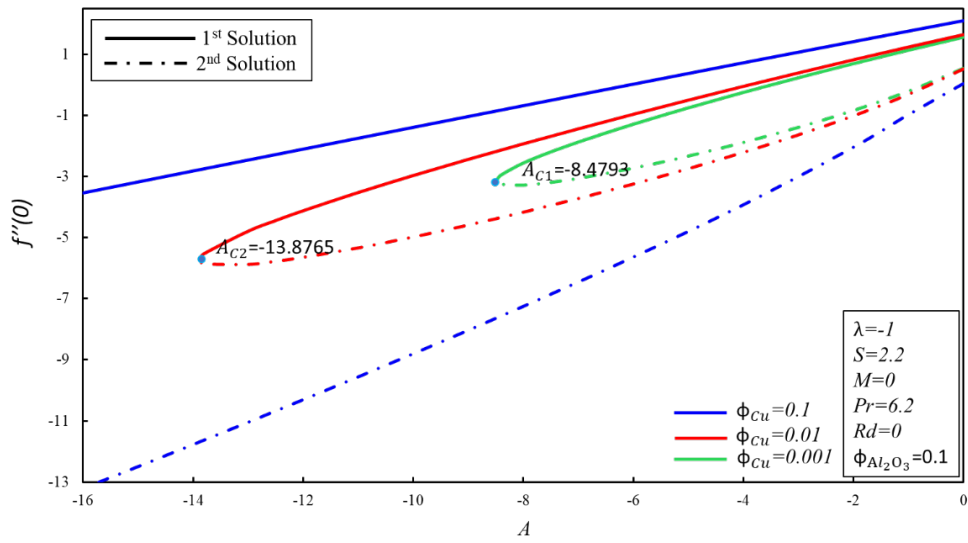
Figure 2. Comparison with the 6th figure of Waini et al. [31].
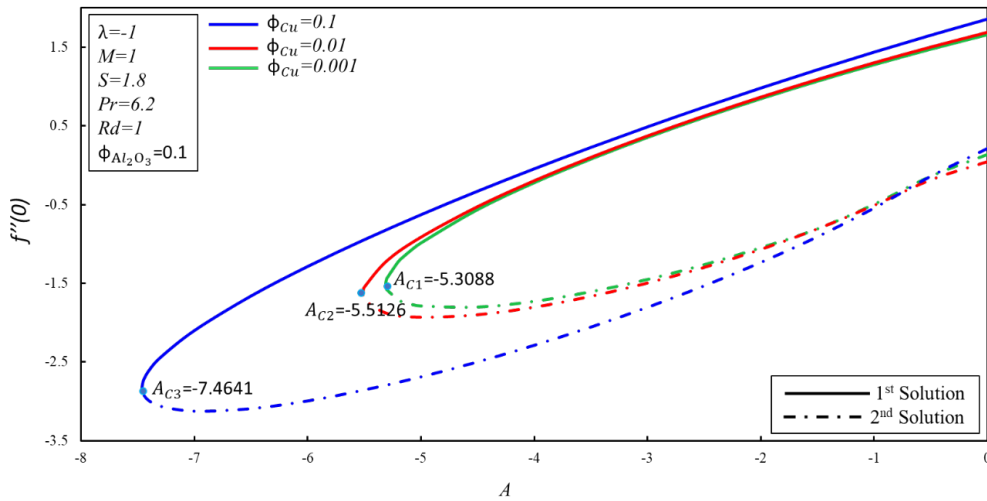
Figure 3. Variation of $f''(0)$ with A for various values of ϕ_{Cu}.
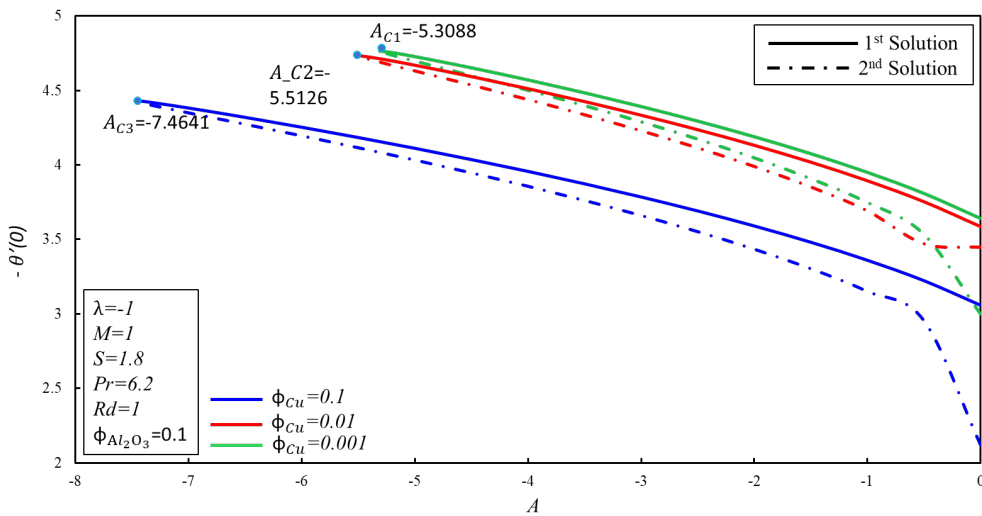
Figure 4. Variation of $-\theta'(0)$ with A for various values of ϕ_{Cu}.
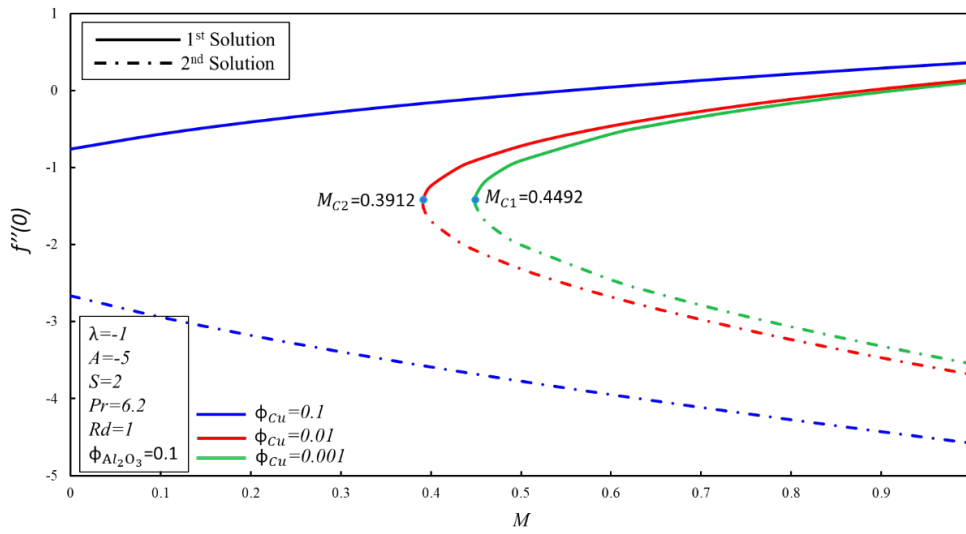
Figure 5. Variation of $f''(0)$ with M for various values of ϕ_{Cu}.
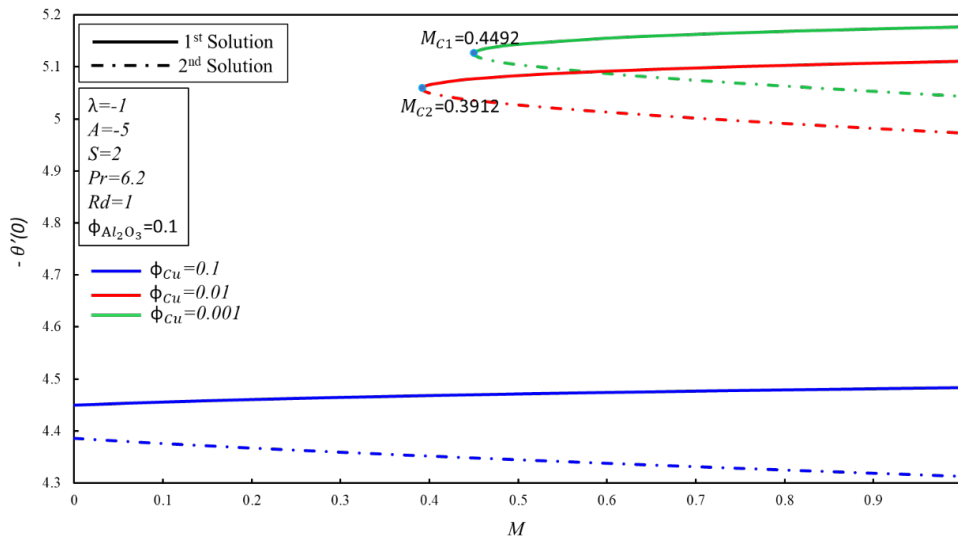
Figure 6. Variation of $-\theta'(0)$ with M for various values of ϕ_{Cu}.
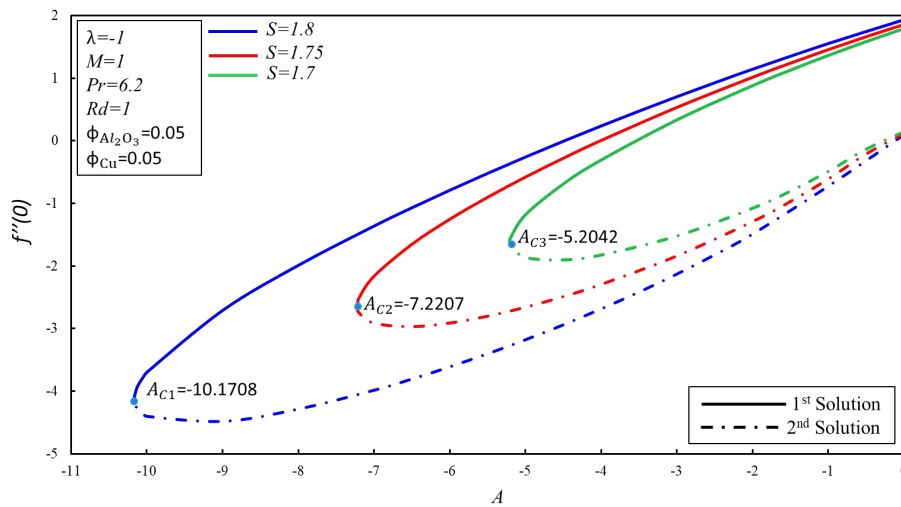
Figure 7. Variation of $f''(0)$ with A for various values of S.
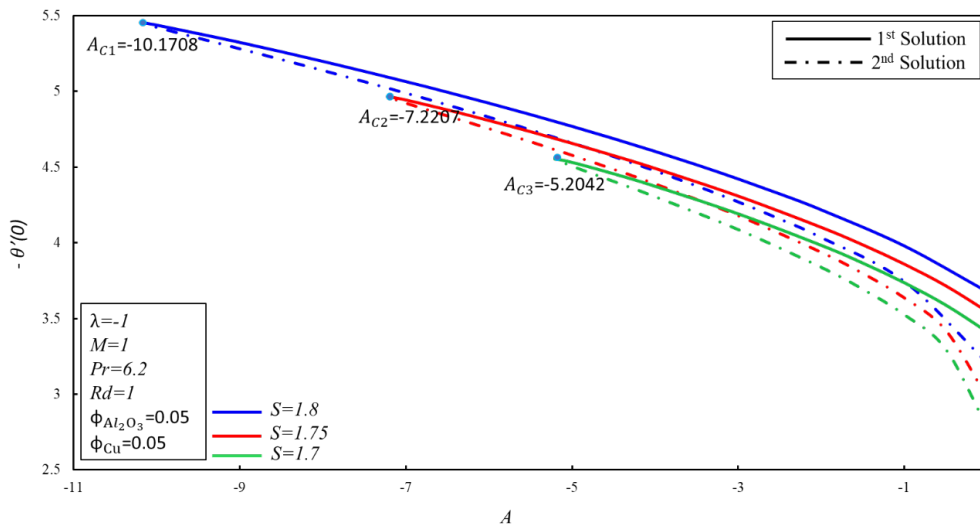
Figure 8. Variation of $-\theta'(0)$ with A for various values of S.
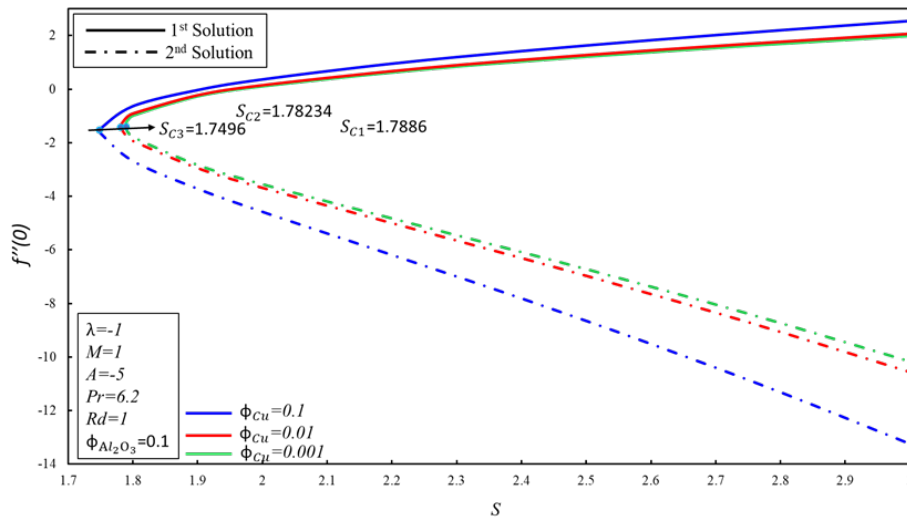
Figure 9. Variation of $f''(0)$ with S for various values of ϕ_{Cu}.
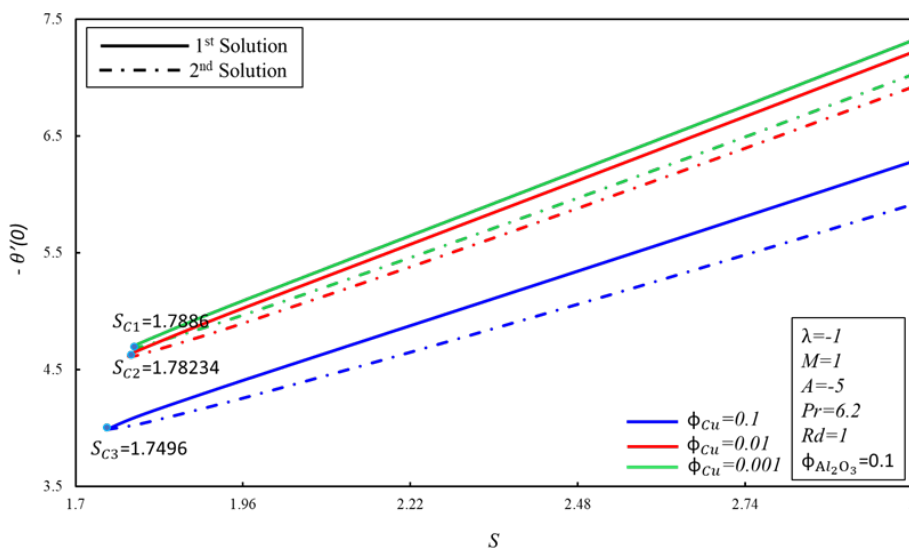
Figure 10. Variation of $-\theta'(0)$ with S for various values of ϕ_{Cu}.
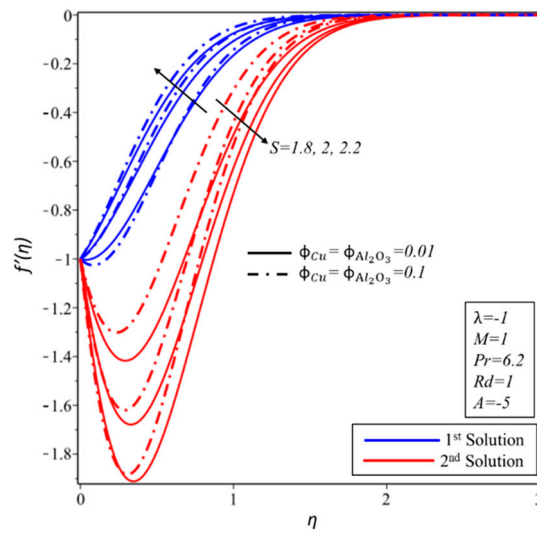
Figure 11. Variation of $f'(\eta)$ with η for various values of S.
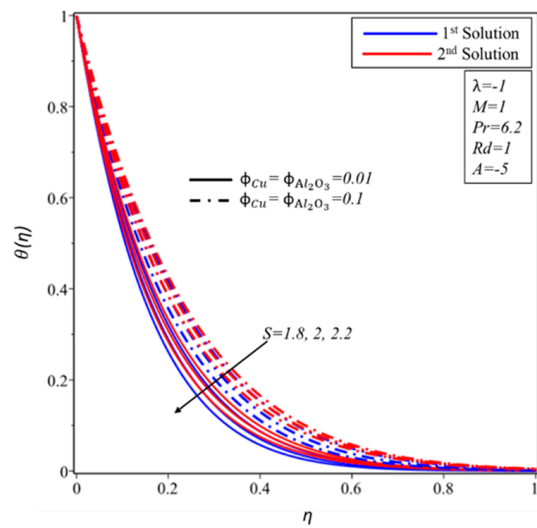
Figure 12. Variation of $\theta(\eta)$ with η for various values of S.
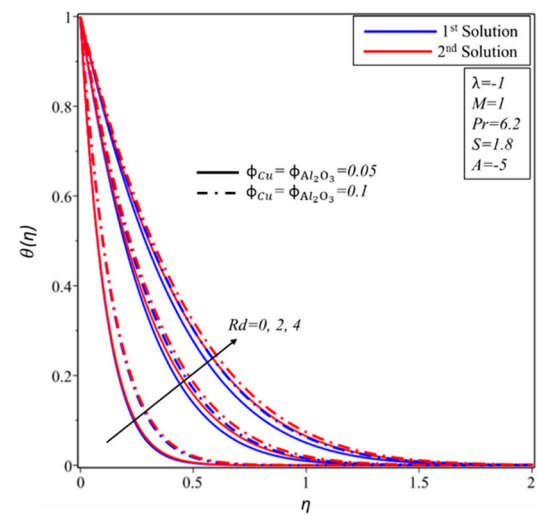
Figure 13. Variation of $\theta(\eta)$ with η for various values of Rd.
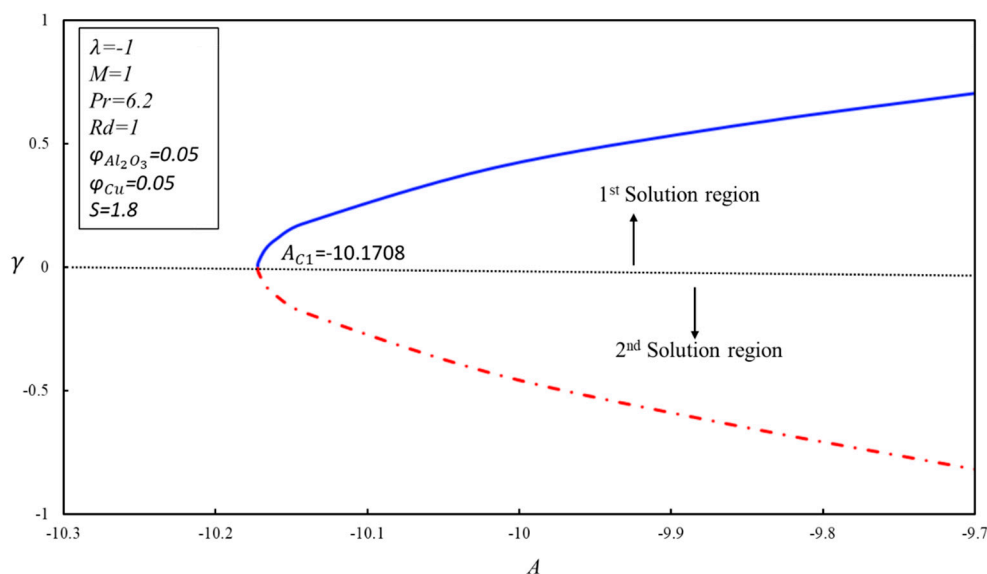
Figure 14. Smallest eigenvalues γ for various values of A.

5. Conclusions

The problem of the unsteady MHD flow of the $Cu - Al_2O_3/$ water hybrid nanofluid in the presence of the thermal radiation effect over the stretching/shrinking sheet is examined. Two methods are adopted to carry out the numerical computations of the current problem, a shooting method is used to get the dual solutions of ODEs (6–8) in MAPLE software 2018, and the computation of the stability analysis is carried out by employing a 3-stage Labatto IIIa formula in a BVP4C solver in MATLAB 2017b. The impacts of ϕ_{Cu} unsteadiness parameter S and suction parameter S on the $f''(0)$, $-\theta'(0)$, $f'(\eta)$, and $\theta(\eta)$ were exhibited graphically and examined. The results show that the development (reduction) of $f''(0)$ and the decline (reduction) of $-\theta'(0)$ past a shrinking sheet is found with the expansion of ϕ_{Cu} in the first (second) solution. The temperature of fluid in both solutions increase (decrease) for the higher values of Rd and S. The fluid velocity decreases when the effect of suction parameter S enhanced in the first solution, whereas it increases in the second solution. Furthermore, it is found that the skin friction coefficient increases with an increase in solid volume friction of ϕ_{Cu} and suction parameter S in the first solution, while it decreases in the second solution. On the other hand, an improvement in the heat transfer rate is noticed when suction parameter S is increased for both solutions, whereas the totally opposite trend is noticed for the case of solid volume friction of ϕ_{Cu}. For the certain ranges of the suction parameter S, unsteadiness parameter A, and magnetic parameter M, dual solutions are noticed. Furthermore, the results of the temporal stability analysis confirm that the first solution is stable, whereas the second solution is unstable. In future, this work can be continued to assess the impact of viscous dissipation, joule heating, boundary slip conditions, and convective boundary conditions. Other than these impacts, it can be extended for three-dimensional boundary layer flows by conserving various possible effects.

Abbreviation

	Nomenclature		
T_0	a constant	$\phi_{Al_2O_3}$	nanoparticle volume fraction of the iron oxide.
T_∞	ambient temperature	M	magnetic parameter
$'$	differentiation with respect to η	K_1	Porous parameter
Rd	Thermal radiation	c	constant
ρ_{hnf}	effective density of hybrid nanofluid	Pr	Prandtl number
ρ_{nf}	effective density of nanofluid	C_f	skin friction coefficient
μ_{hnf}	effective dynamic viscosity of hybrid nanofluid	γ_1	smallest eigen value
μ_{nf}	effective dynamic viscosity of nanofluid	τ	Stability transformed variable
σ^*	electrical conductivity	v_w	suction/injection velocity
f	fluid fraction	T	Temperature
M	Hartmann/magnetic number	k_{hnf}	thermal conductivity of the hybrid nanofluid
$(\rho c_p)_{hnf}$	heat capacitance of the hybrid nanofluid	k_{nf}	thermal conductivity of the nanofluid
$(\rho c_p)_{nf}$	heat capacitance of the nanofluid	t	time
hnf	Hybrid nanofluid	η	transformed variable
N_u	local Nusselt number	A	Unsteadiness parameter
Re	local Reynolds number	T_w	variable temperature at the sheet
B	Magnetic field	u, v	velocity components
nf	nanofluid fraction	λ	shrinking/stretching parameter
k^*	mean absorption coefficient	σ_1	Stefan–Boltzmann constant
ϕ_{Cu}	nanoparticle volume fraction of the copper	S	$S < 0$ for suction parameter and $S > 0$ for blowing parameter

References

1. Choi, S.U.; Eastman, J.A. *Enhancing Thermal Conductivity of Fluids with Nanoparticles*; No. ANL/MSD/CP-84938; CONF-951135-29; Argonne National Lab: Lemont, IL, USA, 1995.
2. Tiwari, R.K.; Das, M.K. Heat transfer augmentation in a two-sided lid-driven differentially heated square cavity utilizing nanofluids. *Int. J. Heat Mass Transf.* **2007**, *50*, 2002–2018. [CrossRef]
3. Benzema, M.; Benkahla, Y.K.; Labsi, N.; Ouyahia, S.E.; El Ganaoui, M. Second law analysis of MHD mixed convection heat transfer in a vented irregular cavity filled with Ag-MgO/water hybrid nanofluid. *J. Therm. Anal. Calorim.* **2019**, *137*, 1113–1132. [CrossRef]
4. Dero, S.; Rohni, A.M.; Saaban, A. The dual solutions and stability analysis of nanofluid flow using tiwari-das modelover a permeable exponentially shrinking surface with partial slip conditions. *J. Eng. Appl. Sci.* **2019**, *14*, 4569–4582. [CrossRef]
5. Lund, L.A.; Omar, Z.; Khan, I.; Dero, S. Multiple solutions of Cu-$C_6H_9NaO_7$ and Ag-$C_6H_9NaO_7$ nanofluids flow over nonlinear shrinking surface. *J. Cent. South Univ.* **2019**, *26*, 1283–1293. [CrossRef]
6. Lund, L.A.; Omar, Z.; Khan, U.; Khan, I.; Baleanu, D.; Nisar, K.S. Stability analysis and dual solutions of micropolar nanofluid over the inclined stretching/shrinking surface with convective boundary condition. *Symmetry* **2020**, *12*, 74. [CrossRef]
7. Dogonchi, A.S.; Chamkha, A.J.; Hashemi-Tilehnoee, M.; Seyyedi, S.M.; Ganji, D.D. Effects of homogeneous-heterogeneous reactions and thermal radiation on magneto-hydrodynamic Cu-water nanofluid flow over an expanding flat plate with non-uniform heat source. *J. Cent. South Univ.* **2019**, *26*, 1161–1171. [CrossRef]
8. Dogonchi, A.S.; Ismael, M.A.; Chamkha, A.J.; Ganji, D.D. Numerical analysis of natural convection of Cu-water nanofluid filling triangular cavity with semicircular bottom wall. *J. Therm. Anal. Calorim.* **2019**, *135*, 3485–3497. [CrossRef]
9. Amini, Y.; Akhavan, S.; Izadpanah, E. Vortex-induced vibration of a cylinder in pulsating nanofluid flow. *J. Therm. Anal. Calorim.* **2019**. [CrossRef]
10. Zaib, A.; Khan, M.; Shafie, S. Boundary-layer flow of a cu-water nanofluid over a permeable shrinking cylinder with homogenous-hetrogenous reactions: Dual solutions. *Therm. Sci.* **2019**, *23*, 295–306. [CrossRef]

11. Raza, J.; Rohni, A.M.; Omar, Z.; Awais, M. Heat and mass transfer analysis of MHD nanofluid flow in a rotating channel with slip effects. *J. Mol. Liq.* **2016**, *219*, 703–708. [CrossRef]

12. Rasool, G.; Zhang, T.; Shafiq, A. Marangoni effect in second grade forced convective flow of water based nanofluid. *J. Adv. Nanotechnol.* **2019**, *1*, 50. [CrossRef]

13. Rasool, G.; Shafiq, A.; Khalique, C.M.; Zhang, T. Magneto-hydrodynamic Darcy-Forchheimer nanofluid flow over nonlinear stretching sheet. *Phys. Scr.* **2019**, *94*, 10. [CrossRef]

14. Dinarvand, S. Nodal/saddle stagnation-point boundary layer flow of CuO-Ag/water hybrid nanofluid: A novel hybridity model. *Microsyst. Technol.* **2019**, *25*, 2609–2623. [CrossRef]

15. Roşca, N.C.; Roşca, A.V.; Pop, I. Unsteady separated stagnation-point flow and heat transfer past a stretching/shrinking sheet in a copper-water nanofluid. *Int. J. Numer. Methods Heat Fluid Flow* **2019**. [CrossRef]

16. Ahmed, N.; Saba, F.; Khan, U.; Mohyud-Din, S.T.; Sherif, E.S.M.; Khan, I. Nonlinear thermal radiation and chemical reaction effects on a Cu-CuO/NaAlg hybrid nanofluid flow past a stretching curved surface. *Processes* **2019**, *7*, 962. [CrossRef]

17. Devi, S.A.; Devi, S.S.U. Numerical investigation of hydromagnetic hybrid Cu-Al_2O_3/water nanofluid flow over a permeable stretching sheet with suction. *Int. J. Nonlinear Sci. Numer. Simul.* **2016**, *17*, 249–257. [CrossRef]

18. Suresh, S.; Venkitaraj, K.P.; Selvakumar, P.; Chandrasekar, M. Synthesis of Al_2O_3-Cu/water hybrid nanofluids using two step method and its thermo physical properties. *Colloids Surf. A Physicochem. Eng. Asp.* **2011**, *388*, 41–48. [CrossRef]

19. Toghraie, D.; Chaharsoghi, V.A.; Afrand, M. Measurement of thermal conductivity of ZnO-TiO_2/EG hybrid nanofluid. *J. Therm. Anal. Calorim.* **2016**, *125*, 527–535. [CrossRef]

20. Moghadassi, A.; Ghomi, E.; Parvizian, F. A numerical study of water based Al_2O_3 and Al_2O_3-Cu hybrid nanofluid effect on forced convective heat transfer. *Int. J. Therm. Sci.* **2015**, *92*, 50–57. [CrossRef]

21. Hayat, T.; Nadeem, S.; Khan, A.U. Rotating flow of Ag-CuO/H_2O hybrid nanofluid with radiation and partial slip boundary effects. *Eur. Phys. J. E* **2018**, *41*, 75. [CrossRef]

22. Saba, F.; Ahmed, N.; Khan, U.; Waheed, A.; Rafiq, M.; Mohyud-Din, S. Thermophysical analysis of water based (Cu-Al_2O_3) hybrid nanofluid in an asymmetric channel with dilating/squeezing walls considering different shapes of nanoparticles. *Appl. Sci.* **2018**, *8*, 1549. [CrossRef]

23. Acharya, N.; Bag, R.; Kundu, P.K. Influence of hall current on radiative nanofluid flow over a spinning disk: A hybrid approach. *Phys. E Low-Dimens. Syst. Nanostruct.* **2019**, *111*, 103–112. [CrossRef]

24. Afridi, M.I.; Alkanhal, T.A.; Qasim, M.; Tlili, I. Entropy Generation in Cu-Al_2O_3-H_2O Hybrid Nanofluid Flow over a Curved Surface with Thermal Dissipation. *Entropy* **2019**, *21*, 941. [CrossRef]

25. Shafiq, A.; Khan, I.; Rasool, G.; Sherif, E.S.M.; Sheikh, A.H. Influence of single-and multi-wall carbon nanotubes on magnetohydrodynamic stagnation point nanofluid flow over variable thicker surface with concave and convex effects. *Mathematics* **2020**, *8*, 104. [CrossRef]

26. Shafiq, A.; Zari, I.; Rasool, G.; Tlili, I.; Khan, T.S. On the MHD casson axisymmetric marangoni forced convective flow of nanofluids. *Mathematics* **2019**, *7*, 1087. [CrossRef]

27. Manh, T.D.; Nam, N.D.; Abdulrahman, G.K.; Moradi, R.; Babazadeh, H. Impact of MHD on hybrid nanomaterial free convective flow within a permeable region. *J. Therm. Anal. Calorim.* **2019**. [CrossRef]

28. Khashi'ie, N.S.; Arifin, N.M.; Nazar, R.; Hafidzuddin, E.H.; Wahi, N.; Pop, I. Magnetohydrodynamics (MHD) axisymmetric flow and heat transfer of a hybrid nanofluid past a radially permeable stretching/shrinking sheet with joule heating. *Chin. J. Phys.* **2019**. [CrossRef]

29. Lund, L.A.; Omar, Z.; Khan, I.; Seikh, A.H.; Sherif, E.S.M.; Nisar, K.S. Stability analysis and multiple solution of Cu-Al_2O_3/H_2O nanofluid contains hybrid nanomaterials over a shrinking surface in the presence of viscous dissipation. *J. Mater. Res. Technol.* **2019**, *9*, 421–432. [CrossRef]

30. Waini, I.; Ishak, A.; Pop, I. Hybrid nanofluid flow and heat transfer past a vertical thin needle with prescribed surface heat flux. *Int. J. Numer. Methods Heat Fluid Flow* **2019**. [CrossRef]

31. Waini, I.; Ishak, A.; Pop, I. Unsteady flow and heat transfer past a stretching/shrinking sheet in a hybrid nanofluid. *Int. J. Heat Mass Transf.* **2019**, *136*, 288–297. [CrossRef]

32. Merkin, J.H. On dual solutions occurring in mixed convection in a porous medium. *J. Eng. Math.* **1986**, *20*, 171–179. [CrossRef]

33. Dero, S.; Rohni, A.M.; Saaban, A.; Khan, I. Dual solutions and stability analysis of micropolar nanofluid flow with slip effect on stretching/shrinking surfaces. *Energies* **2019**, *12*, 4529. [CrossRef]

34. Dero, S.; Uddin, M.J.; Rohni, A.M. Stefan blowing and slip effects on unsteady nanofluid transport past a shrinking sheet: Multiple solutions. *Heat Transf. Asian Res.* **2019**, *6*, 2047–2066. [CrossRef]

35. Lund, L.A.; Omar, Z.; Khan, I. Mathematical analysis of magnetohydrodynamic (MHD) flow of micropolar nanofluid under buoyancy effects past a vertical shrinking surface: Dual solutions. *Heliyon* **2019**, *5*, e02432. [CrossRef]

36. Lund, L.A.; Omar, Z.; Dero, S.; Khan, I. Linear stability analysis of MHD flow of micropolar fluid with thermal radiation and convective boundary condition: Exact solution. *Heat Transf. Asian Res.* **2019**. [CrossRef]

37. Lund, L.A.; Omar, Z.; Khan, I.; Kadry, S.; Rho, S.; Mari, I.A.; Nisar, K.S. Effect of viscous dissipation in heat transfer of MHD flow of micropolar fluid partial slip conditions: Dual solutions and stability analysis. *Energies* **2019**, *12*, 4617. [CrossRef]

38. Lund, L.A.; Omar, Z.; Khan, I.; Raza, J.; Sherif, E.S.M.; Seikh, A.H. Magnetohydrodynamic (MHD) flow of micropolar fluid with effects of viscous dissipation and joule heating over an exponential shrinking sheet: Triple solutions and stability analysis. *Symmetry* **2020**, *12*, 142. [CrossRef]

39. Khashi'ie, N.S.; Arifin, N.M.; Rashidi, M.M.; Hafidzuddin, E.H.; Wahi, N. Magnetohydrodynamics (MHD) stagnation point flow past a shrinking/stretching surface with double stratification effect in a porous medium. *J. Therm. Anal. Calorim.* **2019**. [CrossRef]

40. Waini, I.; Ishak, A.; Pop, I. Transpiration effects on hybrid nanofluid flow and heat transfer over a stretching/shrinking sheet with uniform shear flow. *Alex. Eng. J.* **2019**. [CrossRef]

41. Asma, M.; Othman, W.A.M.; Muhammad, T. Numerical study for darcy-forchheimer flow of nanofluid due to a rotating disk with binary chemical reaction and arrhenius activation energy. *Mathematics* **2019**, *7*, 921. [CrossRef]

42. Alarifi, I.M.; Abokhalil, A.G.; Osman, M.; Lund, L.A.; Ayed, M.B.; Belmabrouk, H.; Tlili, I. MHD flow and heat transfer over vertical stretching sheet with heat sink or source effect. *Symmetry* **2019**, *11*, 297. [CrossRef]

43. Basir, M.F.M.; Kumar, R.; Ismail, A.I.M.; Sarojamma, G.; Narayana, P.S.; Raza, J.; Mahmood, A. Exploration of thermal-diffusion and diffusion-thermal effects on the motion of temperature-dependent viscous fluid conveying microorganism. *Arab. J. Sci. Eng.* **2019**, *44*, 8023–8033. [CrossRef]

44. Wang, Q. Optimal strokes of low Reynolds number linked-sphere swimmers. *Appl. Sci.* **2019**, *9*, 4023. [CrossRef]

45. Iqbal, Z.; Akbar, N.S.; Azhar, E.; Maraj, E.N. Performance of hybrid nanofluid (Cu-CuO/water) on MHD rotating transport in oscillating vertical channel inspired by Hall current and thermal radiation. *Alex. Eng. J.* **2018**, *57*, 1943–1954. [CrossRef]

46. Khashi'ie, N.S.; Arifin, N.M.; Hafidzuddin, E.H.; Wahi, N. Thermally stratified flow of Cu-Al2O3/water hybrid nanofluid past a permeable stretching/shrinking circular cylinder. *J. Adv. Res. Fluid Mech. Therm. Sci.* **2019**, *63*, 154–163.

47. Rahman, A.N.H.; Bachok, N.; Rosali, H. Numerical solutions of MHD stagnation-point flow over an exponentially stretching/shrinking sheet in a nanofluid. In *Journal of Physics: Conference Series*; IOP Publishing: Bristol, UK, 2019; Volume 1366.

48. Zaib, A.; Khan, U.; Shah, Z.; Kumam, P.; Thounthong, P. Optimization of entropy generation in flow of micropolar mixed convective magnetite (Fe_3O_4) ferroparticle over a vertical plate. *Alex. Eng. J.* **2019**, *58*, 1461–1470. [CrossRef]